Abnormal Elastic Changes for Cubic-Tetragonal Transition of Single-Crystal $SrTiO_3$

Caizi Zhang(张才姿)[1], Fangfei Li(李芳菲)[1], Xinmiao Wei(魏鑫苗)[1], Mengqi Guo(郭梦琪)[1], Yingzhan Wei(魏颖展)[1], Liang Li(李亮)[1], Xinyang Li(李新阳)[1*], and Qiang Zhou(周强)[1,2]

[1]*State Key Laboratory of Superhard Materials, Jilin University, Changchun 130012, China*
[2]*Synergetic Extreme Condition User Facility, Jilin University, Changchun 130012, China*

(Received 25 June 2022; accepted manuscript online 1 August 2022)

Strontium titanate ($SrTiO_3$) is a typical perovskite-type ceramic oxide and studying its high-pressure phases are critical to understand the ferroelastic phase transition. $SrTiO_3$ also can be used as an important analog of davemaoite ($CaSiO_3$) to understand the compositional and velocity structure of the Earth's interior. However, the high-pressure studies on the cubic-to-tetragonal phase transition pressure and elastic properties remain unclear for $SrTiO_3$. Here, we investigate the phase transition and elasticity of single-crystal $SrTiO_3$ by Raman and Brillouin scattering combined with diamond anvil cell. The acoustic velocities of single-crystal $SrTiO_3$ and the independent elastic constants of cubic and tetragonal $SrTiO_3$ are determined up to 27.5 GPa at room temperature. This study indicates that C_{11}, C_{12}, and C_{44} exhibit abnormal changes at 10.3 GPa, which is related to the cubic-to-tetragonal phase transition. Interestingly, a significant softening on shear modulus and a large anisotropy of shear wave splitting (A_S^{PO}) jump are observed at 10.3 GPa. Using obtained elastic constants, the coefficients of the Landau potential are calculated to understand the phase transition between cubic and tetragonal. The calculated coefficients of the Landau potential are, $\lambda_2 = 3.12 \times 10^{-2}$ GPa, $\lambda_4 = -2.02 \times 10^{-2}$ GPa, $B^* = 1.34 \times 10^{-4}$ GPa and $B = 1.66 \times 10^{-4}$ GPa. The elastic results have profound implications in understanding the structure of the Earth's interior and indicate that the presence of tetragonal Ti-bearing $CaSiO_3$ helps to explain the large A_S^{PO} of the Earth's mid-mantle.

DOI: 10.1088/0256-307X/39/9/096201

As one of the typical ceramic perovskites, strontium titanate ($SrTiO_3$) has a wide range of technological applications due to its unique ferroelectric, semiconducting and superconducting properties.[1–8] More importantly, $SrTiO_3$ can be used as an analog of Davemaoite ($CaSiO_3$),[9,10] which was discovered as an important mineral from the Earth's lower mantle in recent years.[11,12] Previous studies also indicate that the cubic-to-tetragonal phase transition of (Ca,Ti)SiO_3 could help to explain the observed velocity discontinuity in the Earth's mid-mantle.[13,14] However, the investigation on the elastic properties of $CaSiO_3$ is still limited because the cubic $CaSiO_3$ is a high-pressure phase and quenching the single crystals to ambient conditions is still challenging.[15–17] Both $CaSiO_3$ and $SrTiO_3$ undergo the structural change between $Pm\bar{3}m$ and $I4/mcm$ and $SrTiO_3$ with $Pm\bar{3}m$ space group remains stable under ambient condition.[13,14,18] Thus, the investigation on the phase stability as well as elastic properties of $SrTiO_3$ is key to understand the high-pressure properties of $CaSiO_3$.[13,14] In general, temperature and pressure are the main factors for phase stability. The temperature-induced cubic-to-tetragonal ferroelastic phase transition of $SrTiO_3$ has shown that the temperature of the phase transition is about 105 K.[19,20] With the development of high-pressure experimental technology, numerous studies have demonstrated that pressure can also induce this phase transition of $SrTiO_3$.[18,21–24]

The pressure-induced phase transition has been studied using a variety of methods, including Raman scattering, Brillouin scattering and x-ray diffraction.[18,21–24] Using Raman spectra, Ishidate *et al.*[22] and Grzechnik *et al.*[18] indicated that the cubic-to-tetragonal transition locates around 6 GPa. The Brillouin scattering result of Ishidate *et al.*[23] also showed that the cubic-to-tetragonal phase transition occurs at 6.5 GPa. However, Lheureux *et al.*, who performed a Brillouin scattering study, and Guennou *et al.*, who conducted x-ray diffraction on single-crystal $SrTiO_3$, both indicated that the cubic-to-tetragonal transition would occur above 9 GPa.[21,24] Such differences between these transition pressures in different groups is unclear till now. The *ab initio* pseudo-potential calculation indicated that the bulk and shear moduli of $SrTiO_3$ would decrease at the critical point, suggesting that the cubic-to-tetragonal phase transition has a certain effect on the elastic modulus,[25] but without any thermal expansion or the dielectric constant changes.[26,27] Thus, to get more clear insights into the pressure-induced cubic-to-tetragonal transitional mechanism, we performed *in situ* Raman and Brillouin scattering of single-crystal $SrTiO_3$ up to 27.5 GPa at 298 K. The determined elastic properties display clearly abnormal changes between the cubic-tetragonal transition of $SrTiO_3$. The elastic results have profound implications for understanding the high anisotropy zones in the Earth's mid-mantle.

The single-crystal $SrTiO_3$ with (100) crystallographic orientation from Prmat (Shanghai) Technology Co., Ltd was used in this work. We polished both sides of the crys-

*Corresponding authors. Email: lixinyang@jlu.edu.cn
© 2022 Chinese Physical Society and IOP Publishing Ltd

tal to 30 μm by Al_2O_3 lapping discs and the crystal was cut into $80 \times 80\,\mu m^2$. The crystallographic orientation of the polished single crystal is (0.98, 0.16, 0.08). The x-ray diffraction measurement illustrated that the single-crystal $SrTiO_3$ is cubic structure with $Pm\bar{3}m$ space group and the unit-cell parameter is $a = 3.910(1)$ Å. The density under ambient condition is $\rho = 5.099(3)\,g/cm^3$. The diamond anvil cell (DAC) equipped with a pair of diamonds with 400 μm culet was used to perform the high-pressure experiment. The sample chamber is a T301 stainless steel gasket, which was pre-indented to 50 μm and a 200 μm hole was drilled at the center of the indentation. A ruby sphere was loaded into the hole as the pressure indicator.[28] Argon was used as the pressure transmitting medium.

Brillouin scattering signal was collected with a 3+3 Tandem Fabry–Pérot Interferometer by employing the symmetric platelet (50°) scattering geometries.[29] The excitation source is a single frequency 532 nm laser. The source power is 140 mW and the power on the sample is 40 mW. The acoustic velocity is calculated by

$$v = \frac{\Delta\omega\lambda_0}{2\sin(\theta/2)}, \tag{1}$$

where v is the acoustic velocity, $\Delta\omega$ is the Brillouin frequency shift, λ_0 is the wavelength of the incident beam, and θ is the external scattering angle. The refractive index is ignored in the acoustic velocity calculation since Whitfield *et al.*[30] demonstrated that the acoustic velocity can also be calculated in the platelet geometry without considering the refractive index. At each pressure, the DAC was kept for one night to stabilize the pressure in the sample chamber. The Raman scattering was performed with a Raman spectrometer (HRS-750) after Brillouin scattering measurement at each pressure. The wavelength of the excitation laser is 532 nm, and the source power is 10 mW. The Raman spectra were collected in a backscattering geometry.

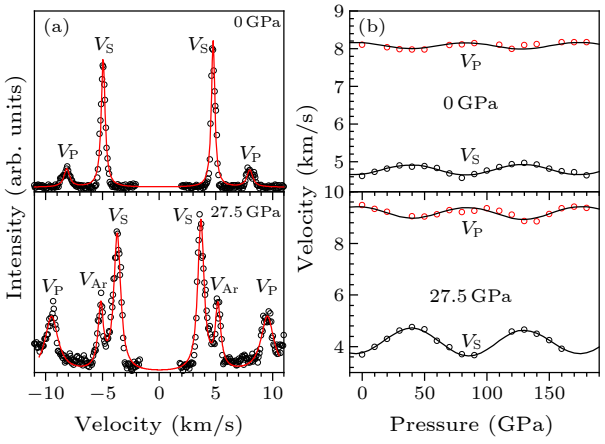

Fig. 1. (a) Representative Brillouin spectra at 0 GPa and 27.5 GPa. (b) Measured velocities as a function of azimuthal angles for (0.98, 0.16, 0.08) at 0 GPa and 27.5 GPa. The open circle is the experimental data, and the solid line is the fitting result.

Figure 1(a) shows the representative Brillouin scattering spectra of the single-crystal $SrTiO_3$ under ambient condition and high pressure. The longitudinal velocities and shear velocities of the single-crystal $SrTiO_3$ were detected at each pressure as shown in Fig. 1(a). Since the single crystal is anisotropic, we collected the Brillouin spectra from 0° to 180° with an interval of 10° at each pressure to obtain sufficient elastic information of the single-crystal $SrTiO_3$. The velocities as a function of azimuthal angles are shown in Fig. 1(b). The elastic constants C_{ij} are calculated by Christoffel's equation[31]

$$|C_{ijkl}n_jn_l - \rho v^2\delta_{ik}| = 0, \tag{2}$$

where n_j and n_l represent the direction cosines of the phonon along the propagation direction; δ_{ik} is the Kronecker delta function; C_{ijkl} is the elastic constant, abbreviated as C_{ij} in this study; ρ is the density at each pressure. The high-pressure density used here is taken from Ref. [21].

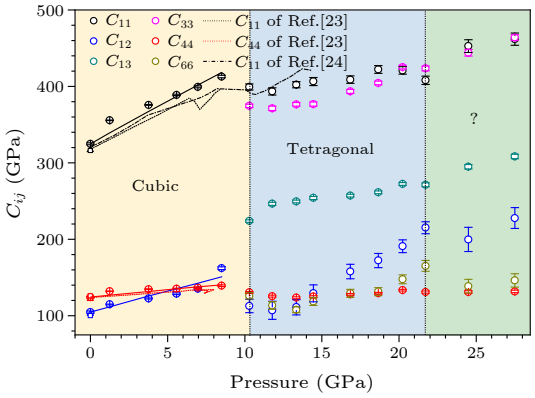

Fig. 2. Elastic constants of single-crystal $SrTiO_3$ at high pressures. The open circles indicate the results of this study. The open rectangles and the open triangles are the experimental results under ambient condition from Refs. [23,32], respectively. The dotted lines are the high-pressure elastic constants in Ref. [23], the black one represents C_{11} and the red one represents C_{44}. The dashed-dotted line represents the high-pressure C_{11} in Ref. [24]. The solid lines are the results of three-order finite strain equation fitting. The background with different colors represents the single-crystal $SrTiO_3$ in different phases. Yellow represents the cubic phase, blue represents the tetragonal phase, and green represents the unknown phase.

$SrTiO_3$ in cubic structure has 3 independent elastic constants C_{11}, C_{12}, and C_{44}. The calculated elastic constants at high pressure are presented in Fig. 2 and Table 1. The elastic constants under ambient condition of this study are in good agreement with the previous experimental results.[23,32] Under high pressure conditions, C_{11} also agrees well with Ref. [24] within the uncertainty. As shown in Fig. 2, C_{11} is larger than C_{44} and C_{12}, indicating the most incompressibility along the a, b, c axes. The pressure derivatives (C'_{ijkl}) of the elastic constants are obtained by fitting the experimental results and three-order finite strain equation:[33]

$$C_{ijkl}(f) = (1+2f)^{7/2}(C^0_{ijkl} + b_1 f) - P\Delta_{ijkl}, \tag{3}$$

$$f = \frac{1}{2}[(V_0/V)^{2/3} - 1], \tag{4}$$

$$b_1 = 3K_0(C'_{ijkl} + \Delta_{ijkl}) - 7C^0_{ijkl}, \tag{5}$$

$$\Delta_{ijkl} = -\delta_{ij}\delta_{kl} - \delta_{ik}\delta_{jl} - \delta_{il}\delta_{jk}, \tag{6}$$

where C_{ijkl} represents the elastic at each pressure; f is the finite strain; V_0 is the unit cell volume under ambient

condition; V is the unit cell volume at high pressure; P is the pressure; C^0_{ijkl} and K_0 are the elastic constants and bulk modulus under ambient condition, δ is the Kronecker index, Δ is taken as -3, -1, and -1 for C_{11}, C_{12}, and C_{44}, respectively. Therefore, the pressure derivatives of the elastic constants in cubic phase are obtained as follows: $C'_{11} = 10.9(6)$, $C'_{12} = 5.3(5)$, and $C'_{44} = 2.0(2)$, which indicates that C_{11} increases faster than C_{44} and C_{12} with increasing pressure.

Table 1. Elastic moduli of single-crystal $SrTiO_3$ at high pressure and 298 K.

P (GPa)	ρ (g/cm^3)	C_{11} (GPa)	C_{12} (GPa)	C_{44} (GPa)	C_{13} (GPa)	C_{33} (GPa)	C_{66} (GPa)	K_S (GPa)	G (GPa)	V_P (km/s)	V_S (km/s)	A_P (%)	A_S^{PO} (%)	Poisson's ratio (ν)
0	5.099 (3)	325 (1)	105 (1)	124 (1)				178 (1)	118 (1)	8.10 (1)	4.83 (1)	2.78 (1)	5.91 (1)	0.228 (1)
1.3	5.146*	356 (1)	115 (1)	132 (1)				195 (1)	127 (1)	8.41 (1)	4.99 (1)	2.07 (1)	4.46 (1)	0.232 (1)
3.8	5.218*	376 (1)	123 (1)	135 (1)				207 (1)	131 (1)	8.55 (1)	5.03 (1)	1.40 (1)	3.07 (1)	0.238 (1)
5.6	5.267*	389 (1)	129 (1)	135 (1)				216 (1)	133 (1)	8.63 (1)	5.03 (1)	0.92 (1)	2.04 (1)	0.244 (1)
7.0	5.302*	399 (1)	135 (2)	137 (1)				223 (1)	135 (1)	8.71 (1)	5.05 (1)	0.74 (1)	1.66 (1)	0.249 (1)
8.5	5.341*	413 (2)	162 (2)	139 (1)				246 (1)	133 (1)	8.90 (1)	5.02 (1)	2.19 (1)	5.23 (1)	0.270 (1)
10.3	5.591*	399 (4)	113 (9)	131 (1)	224 (2)	374 (2)	126 (4)	253 (2)	112 (1)	8.40 (2)	4.50 (2)	7.67 (2)	26.98 (2)	0.306 (2)
11.8	5.620*	393 (5)	107 (17)	126 (1)	247 (2)	371 (3)	114 (5)	256 (3)	100 (1)	8.36 (4)	4.31 (3)	9.41 (4)	36.43 (3)	0.328 (3)
13.4	5.650*	402 (4)	111 (10)	124 (1)	249 (2)	377 (2)	108 (4)	262 (3)	99 (1)	8.38 (3)	4.29 (2)	9.12 (3)	35.62 (2)	0.331 (2)
14.4	5.670*	406 (5)	129 (11)	125 (1)	254 (2)	377 (3)	119 (5)	270 (3)	101 (1)	8.44 (3)	4.32 (3)	8.69 (3)	33.46 (3)	0.333 (2)
16.9	5.714*	409 (5)	158 (9)	128 (1)	257 (2)	394 (3)	129 (5)	282 (2)	107 (1)	8.54 (3)	4.37 (2)	7.61 (3)	26.97 (2)	0.332 (2)
18.7	5.746*	422 (5)	172 (9)	130 (1)	261 (2)	405 (2)	132 (5)	292 (2)	110 (1)	8.64 (2)	4.40 (2)	7.37 (2)	25.37 (2)	0.333 (2)
20.2	5.773*	421 (5)	191 (8)	134 (1)	272 (2)	425 (2)	148 (6)	302 (2)	113 (1)	8.79 (2)	4.46 (2)	7.60 (2)	29.34 (2)	0.334 (2)
21.7	5.798*	408 (5)	215 (8)	131 (1)	271 (3)	424 (3)	165 (7)	305 (2)	112 (1)	8.77 (2)	4.42 (2)	9.66 (2)	34.49 (2)	0.337 (2)
24.5	5.844*	453 (8)	200 (16)	131 (2)	295 (3)	444 (4)	139 (9)	323 (3)	112 (2)	8.94 (4)	4.42 (3)	6.54 (4)	26.42 (3)	0.345 (3)
27.5	5.892*	462 (8)	228 (14)	132 (2)	308 (3)	464 (4)	146 (9)	340 (3)	113 (2)	9.06 (3)	4.42 (3)	6.44 (3)	27.71 (3)	0.350 (2)

*The high-pressure density is obtained from Ref. [21].

Table 2. Transition pressure, pressure medium and experimental methods for the high-pressure studies of single-crystal $SrTiO_3$.

Experimental technique	Pressure transmitting medium	Phase transition pressure	References
Brillouin scattering	Unknown	9 GPa	Lheureux *et al.* [24]
	4:1 mixture of methanol and ethanol	6.5 GPa	Ishidate *et al.* [23]
	Argon	10.3 GPa	This study
Raman scattering	4:1 mixture of methanol and ethanol	6.4 GPa	Ishidate *et al.* [22]
	CsI	6 GPa	Grzechnik *et al.* [18]
	Neon	9.5 GPa	Guennou *et al.* [21]
	Argon	10.3 GPa	This study
X-ray Diffraction	Neon	9.5 GPa	Guennou *et al.* [21]

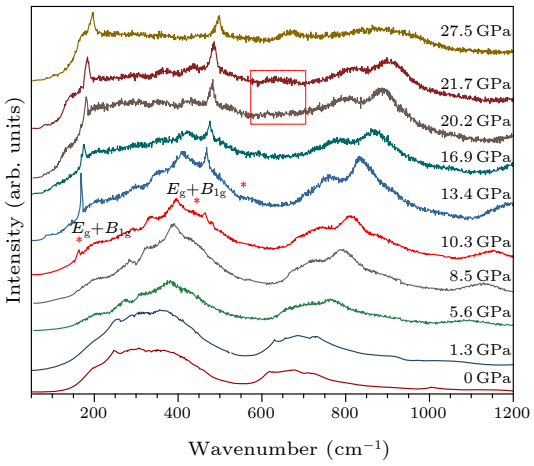

Fig. 3. Representative Raman spectra of $SrTiO_3$ as a function of pressure at room temperature. The stars indicate a new phase which appears at 10.3 GPa. The width of the peak in the dotted rectangle shows an obvious broadening at 21.7 GPa.

The representative Raman spectra of single-crystal $SrTiO_3$ at high pressures are shown in Fig. 3. Under ambient condition, the Raman spectrum of the single-crystal $SrTiO_3$ exhibits two broad bands around 350 cm^{-1} and 650 cm^{-1}, which is consistent with the previous studies.[18,21] Two broad bands sharpen and split with increasing pressure. At 10.3 GPa, two new peaks emerge at 165 cm^{-1} and 465 cm^{-1}, indicating a cubic-to-tetragonal phase transition. The new peaks are attributed to the E_g and B_{1g} modes of the tetragonal phase, respectively. In addition to these two peaks, a new peak at 570 cm^{-1} is also discovered at 13.4 GPa. With increasing pressure, there are no other anomalous changes in the Raman spectra until 21.7 GPa, where the Raman peak at 570 cm^{-1} broadens, and this is consistent with the pressure regime of the observed elastic discontinuities (Fig. 2).

The transition pressure between cubic and tetragonal for single-crystal $SrTiO_3$ still remains controversial in the previous studies.[18,21–24] To better understand the phase transition, we summarize the phase transition pressure, pressure medium and experimental methods of previous studies and this study in Table 3. The studies used methanol-ethanol (4:1) and CsI as the pressure medium indicate that the phase transition pressure is around 6 GPa. However, the transition pressure is around 9.5 GPa when the pressure medium is noble gases (neon, argon) (Table 2). We should note that the transition pressure in this study is 10.3 GPa, which is higher than 9.5 GPa. The experimental pressure step is ∼2 GPa in this study, resulting in the lacking of datasets between 8.5 and 10.3 GPa. Therefore, the transition pressure should be closer to 9.5 GPa in this study. In the high-pressure experiments, the noble gases could maintain a quasi-hydrostatic condition better than the solid pressure medium.[34] Thus, the phase transition of single-crystal $SrTiO_3$ should be af-

fected by the internal stress in the DAC and the non-quasi-hydrostatic condition may shift the transition to lower pressure.

At 10.3 GPa, taking into account the lattice symmetry of the tetragonal phase, six independent elastic constants C_{11}, C_{12}, C_{44}, C_{13}, C_{33}, and C_{66} are used to fit Christoffel's equation in the tetragonal phase.[35] In comparison with the cubic phase, C_{11}, C_{44}, and C_{12} decrease by 3%, 6%, and 30% for tetragonal phase at 10.3 GPa, respectively. The decrease in C_{11} illustrates that the compression along a and c axes in the tetragonal phase is easier than that in the cubic phase. C_{11} is larger than C_{33}, indicates that the c axis has the largest compressibility in the tetragonal phase. The phase transition has the least effect on C_{44}, indicating that the phase transition has negligible effect on shear along the (100) plane.

Table 3. Coefficients of the Landau potential.

	Ambient pressure (Ref. [9])	9.6 GPa (Ref. [21])	9.6 GPa (this study)	
A	1.8×10^{-5}	1.8×10^{-5}	1.8×10^{-5}	GPa/K
Θ_S	60.8	60.8	60.8	K
T_C	105.6	105.6	105.6	K
B	1.2281×10^{-3}	9.2×10^{-5}	1.66×10^{-4}	GPa
B^*	8.1×10^{-4}	7.6×10^{-5}	1.34×10^{-4}	GPa
C	1.092×10^{-3}			GPa
λ_2	4.6×10^{-2}	3.07×10^{-2}	3.12×10^{-2}	GPa
λ_4	-7.5×10^{-2}	-1.15×10^{-2}	-2.02×10^{-2}	GPa
$(C_{11}+2C_{12})/3$	180	230	248	GPa
$(C_{11}-C_{12})/2$	114	135	137	GPa

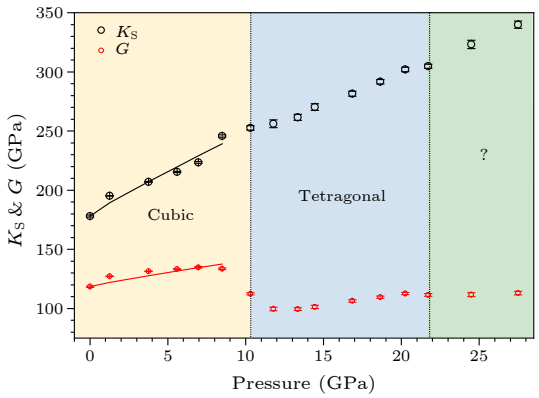

Fig. 4. Bulk modulus K_S and shear modulus G as a function of pressure. The solid lines represent the fitting results of third-order finite strain equation. The background with different colors represents the different phases of single-crystal $SrTiO_3$. Yellow represents the cubic phase, blue represents the tetragonal phase, and green represents the unknown phase.

For tetragonal phase of $SrTiO_3$, C_{11} and C_{33} slightly decrease between 10.3 GPa and 11.8 GPa then keep increasing up to 27.5 GPa. C_{11} is greater than C_{33} between 11.8 GPa and 14.4 GPa but C_{11} nearly equals C_{33} between 16.9 GPa and 20.2 GPa, indicating that the compressibility along (001) plane increases faster than (100) plane. C_{44} and C_{66} slightly decrease between 10.3 GPa and 13.4 GPa. C_{12} also slightly decreases between 10.3 GPa and 11.8 GPa. C_{13} increases with the pressure from 10.3 GPa to 21.7 GPa. C_{12} greatly increases with pressure from 13.4 GPa to 21.7 GPa. Except for the pressure at 20.2 GPa and 21.7 GPa, C_{44} and C_{66} remain equal between 14.9 GPa and 21.7 GPa, indicating that the (100) and (001) planes have similar shear properties at those pressures. The decreases of C_{11}, C_{33}, C_{44}, C_{66}, and C_{12} between 10.3–11.8 GPa are related to the bending of the Ti–O bond and the inhibition of the off-center dynamic distortions at the Ti^{4+} cation sites caused by the cubic-to-tetragonal phase transition.[18] Previous study has observed a weak band splitting at 15.5 GPa,[18] and the splitting was thought to be caused by a tetragonal-orthorhombic phase transition. However, that transition was not detected by the high-pressure x-ray diffraction of single-crystal $SrTiO_3$.[21] Thus, we suppose that the increase of C_{ij} may indicate that the dynamic distortions of TiO_6 octahedra are completed above 14.9 GPa. In other words, the dynamic distortion of TiO_6 octahedra caused by the cubic-tetragonal phase transition starts at 10.3 GPa and finishes at 13.4 GPa, which is consistent with Brillouin and Raman results.

In addition, C_{11} and C_{33} show slight changes at 21.7 GPa. Then C_{12} and C_{66} are significantly decreased by 7% and 16% at 24.5 GPa. The previous experimental study[21] did not observe the structural change under this condition. However, the Raman result in this study shows broadening of the peak at 570 cm^{-1} under 21.7 GPa. Thus, we suppose that single-crystal should have a structural transition at 21.7 GPa. The transition may be the second-order phase transition which is related to the locally structural changes,[21,36] or, it may be caused by the predicted tetragonal-orthorhombic phase transition.[18,25] Raman peak broadening is usually related to the partial collapse of translational long-range order and local atomic displacements.[37–40] Thus, the abnormal changes in elasticity and the broadening of Raman peaks may be related to displacements of the Sr atom.[18] However, we cannot get the specific structural information due to lacking of XRD data, and this transition needs to be further investigated in the future.

Bulk modulus K_S and shear modulus G are also calculated at high pressure (Fig. 4). For the single crystal with cubic structure, according to the elastic moduli obtained above, the K_S and G are calculated by

$$K_S = \frac{1}{3}(C_{11} + 2C_{12}), \tag{7}$$

$$G_{\rm Voigt} = \frac{1}{5}(C_{11} - C_{12} + 3C_{44}), \tag{8}$$

$$G_{\rm Reuss} = \frac{5(C_{11} - C_{12})C_{44}}{4C_{44} + 3(C_{11} - C_{12})}, \tag{9}$$

where $G_{\rm Voigt}$ and $G_{\rm Reuss}$ are the Voigt and Reuss limits of the shear modulus, respectively.[41] The shear modulus is the arithmetic mean value of the two bounds, which is called the Voigt–Reuss–Hill (VRH) average:

$$G = (G_{\rm Voigt} + G_{\rm Reuss})/2. \tag{10}$$

For the single crystal with tetragonal structure, the $K_{\rm S}$ and G are calculated using the following equations:

$$K_{\rm S,Voigt} = \frac{1}{9}[2(C_{11} + C_{12}) + C_{33} + 4C_{13}], \tag{11}$$

$$K_{\rm S,Reuss} = \frac{C^2}{M}, \tag{12}$$

$$G_{\rm Voigt} = \frac{1}{30}[M + 3(C_{11} - C_{12}) + 12C_{44} + 6C_{66}], \tag{13}$$

$$G_{\rm Reuss} = 15\Big[\frac{18K_{\rm S,Voigt}}{C^2} + \frac{6}{C_{11} - C_{12}} + \frac{6}{C_{44}} + \frac{3}{C_{66}}\Big]^{-1}, \tag{14}$$

$$M = C_{11} + C_{12} + 2C_{33} - 4C_{13}, \tag{15}$$

$$C^2 = (C_{11} + C_{12})C_{33} - 2C_{13}^2, \tag{16}$$

where $K_{\rm S,Voigt}$ and $G_{\rm Voigt}$ are the Voigt bound, $K_{\rm S,Reuss}$ and $G_{\rm Reuss}$ are the Reuss bound of the $K_{\rm S}$ and G.[41] The pressure derivatives of the elastic modulus in cubic phase can be obtained by fitting the three-order finite strain equation:

$$K = K_0(1 + 2f)^{5/2}[1 + (K' - 5)f], \tag{17}$$

$$G = (1 + 2f)^{5/2}[G_0 + (3K_0G' - 5G_0)f], \tag{18}$$

where K and G are the bulk modulus and shear modulus at each pressure; f is the finite strain [Eq. (4)]. K_0 is the bulk modulus under ambient condition. K' and G' are the pressure derivatives of bulk modulus and shear modulus, respectively. In the cubic phase, the pressure derivatives are $K' = 6.8(4)$ and $G' = 2.2(2)$. The $K_{\rm S}$ increases with pressure and $K_{\rm S}$ gradient slightly changes at 10.3 GPa due to the cubic-tetragonal transition. The G increases with pressure below 10.3 GPa and presents a significant softening at 10.3 GPa, which is also related to the cubic-tetragonal transition.

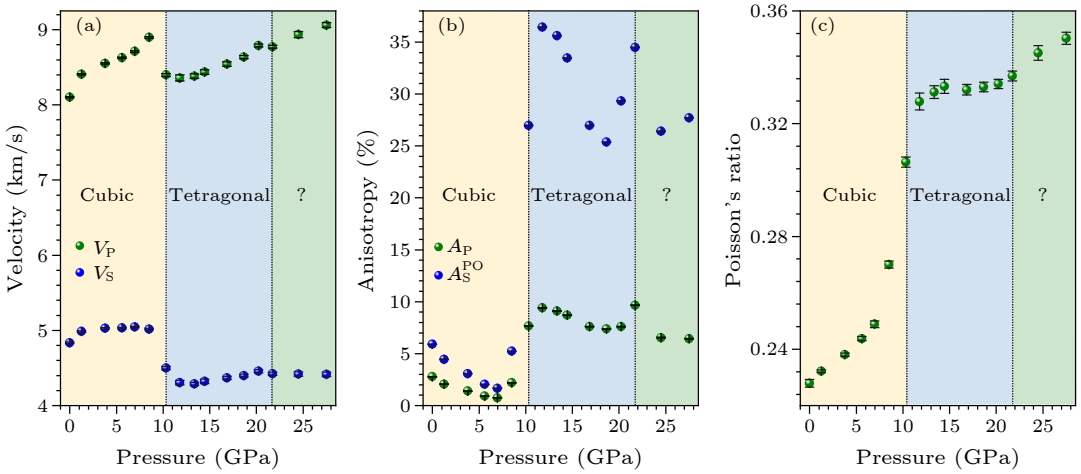

Fig. 5. (a) Aggregate velocity calculated from the elastic modulus. The green solid circles are compressional wave velocity ($V_{\rm P}$) and the blue solid circles are shear wave velocity ($V_{\rm S}$). (b) Velocity anisotropy. The green solid circle is compressional wave anisotropy ($A_{\rm P}$) and the blue solid circle is anisotropy of $V_{\rm S}$ splitting ($A_{\rm S}^{\rm PO}$). (c) Poisson's ratio (ν) of the single-crystal $SrTiO_3$. The background with different colors represents the different phases of single-crystal $SrTiO_3$. Yellow represents the cubic phase, blue denotes the tetragonal phase, and green stands for the unknown phase.

The compressional wave velocity $V_{\rm P}$ and shear wave velocity $V_{\rm S}$ are calculated by using the following equation:

$$V_{\rm P}^2 = \frac{1}{\rho}\Big(K_{\rm S} + \frac{4}{3}G\Big), \tag{19}$$

$$V_{\rm S}^2 = \frac{G}{\rho}, \tag{20}$$

where ρ is the density at each pressure. The data of high-pressure density are taken from Ref. [21]. $V_{\rm P}$ increases with pressure and softens at 10.3 GPa and 21.7 GPa due to the phase transition. However, $V_{\rm S}$ remains unchangeable with increasing pressure below 10.3 GPa but exhibits significantly softening when the cubic-to-tetragonal phase transition occurs at 10.3 GPa [Fig. 5(a)]. The $V_{\rm P}$ and $V_{\rm S}$ drop by 6% and 10% in the cubic-to-tetragonal phase transition at 10.3 GPa, respectively [Fig. 5(a)]. The compressional wave anisotropy ($A_{\rm P}$), anisotropy of shear wave splitting ($A_{\rm S}^{\rm PO}$) and Poisson's ratio (ν) (Fig. 5) are also calculated by

$$A_{\rm P} = \frac{V_{\rm Pmax} - V_{\rm Pmin}}{V_{\rm Pavg}}, \tag{21}$$

$$A_{\rm S}^{\rm PO} = \frac{\max(V_{\rm S2} - V_{\rm S1})}{V_{\rm Savg}}, \tag{22}$$

$$\nu = \frac{3K_{\rm S} - 2G}{2(3K_{\rm S} + G)}, \tag{23}$$

where $V_{\rm Pmax}$ is the maximum of compressional wave, $V_{\rm Pmin}$ is the minimum of compressional wave velocity, $V_{\rm Pavg}$ is the average of compressional wave velocity; $\max(V_{\rm S2} - V_{\rm S1})$ indicates the largest difference between the fast shear wave velocity ($V_{\rm S2}$) and slow shear wave velocity ($V_{\rm S1}$) in a same

azimuthal angle, and $V_{\rm Savg}$ is the average shear wave velocity in the same azimuthal angle. Results indicate that the cubic-to-tetragonal transition also has significant effects on the $A_{\rm P}$, $A_{\rm S}^{\rm PO}$, and ν of $SrTiO_3$. This transition increases the $A_{\rm P}$, $A_{\rm S}^{\rm PO}$, and ν by 5.5%, 21.7%, and 7% [Figs. 5(b) and 5(c)].

The softening of G and $V_{\rm S}$ is commonly thought of as a precursor to the transition from high symmetry to low symmetry.[42–44] The cubic-to-tetragonal ferroelastic transition should be driven by the tilt of the TiO_6 octahedra.[9,45] To better understand the phase transition and the tilt of TiO_6 octahedra, Landau theoretical framework can be used to characterize the elastic anomaly generated by the phase transition.[9,21,46–50] Landau potential can be expressed as[9]

$$\begin{aligned} G = {} & \frac{1}{2}A\Theta_{\rm S}\Big[\coth\frac{\Theta_{\rm S}}{T} - \coth\frac{\Theta_{\rm S}}{T_{\rm C}}\Big]Q^2 + \frac{1}{4}BQ^4 + \frac{1}{6}CQ^6 \\ & + \lambda_2 e_a Q^2 + 2\lambda_4 e_t Q^2 + \frac{1}{4}(C_{11}^0 - C_{12}^0)e_t^2 \\ & + \frac{1}{6}(C_{11}^0 + 2C_{12}^0)e_a^2 + Pe_a, \end{aligned} \tag{24}$$

where A, B, and C are the Landau potential coefficients, Q represents the order parameters, $\Theta_{\rm S}$ is the saturation temperature representing the quantum saturation effect,[51] C_{ij}^0 is the bare elastic constant under ambient condition; λ_2 and λ_4 denote the coupling coefficients between the order parameter and the spontaneous strains; $T_{\rm C}$ is the critical temperature point of the phase transition; e_a and e_t are the volume and tetragonal spontaneous strains, which are related to the lattice parameters by

$$e_a = 2e_1 + e_3, \tag{25}$$

$$e_t = \frac{2(e_3 - e_2)}{\sqrt{3}}, \tag{26}$$

$$e_1 = e_2 = \frac{a_{\rm pc} - a_0}{a_0}, \tag{27}$$

$$e_3 = \frac{c_{\rm pc} - a_0}{a_0}, \tag{28}$$

where e_1, e_2, and e_3 are the spontaneous strain components along the a, b, and c axes for the cubic phase, $a_{\rm pc}$ and $c_{\rm pc}$ are the pseudocubic lattice constants, and a_0 is the cubic phase lattice constant at each pressure.

A simplified Landau model can be used for the pressure-induced phase transition (see the Supplementary Material).[21] Then the volume strain and tetragonal strain as a function of pressure are expressed as

$$e_a = -2\Big[\frac{\lambda_2}{\frac{1}{3}(C_{11}^0 + 2C_{12}^0)}\Big]^2\Big[\frac{P - P_{\rm C}}{B^*}\Big], \tag{29}$$

$$e_t = -4\Big[\frac{\lambda_4}{\frac{1}{2}(C_{11}^0 - C_{12}^0)}\Big]\Big[\frac{\lambda_2}{\frac{1}{3}(C_{11}^0 + 2C_{12}^0)}\Big]\Big[\frac{P - P_{\rm C}}{B^*}\Big], \tag{30}$$

where B^* is the renormalized coefficient in the 246 Landau potential (se the Supplementary Material)[21] and $P_{\rm C}$ is the critical point pressure of the cubic-to-tetragonal phase transition. Then the λ_4 can be obtained by

$$\frac{\partial e_t/\partial P}{\partial e_a/\partial P} = \frac{2(\lambda_4/\lambda_2)[\frac{1}{3}(C_{11} + 2C_{12})]}{[\frac{1}{2}(C_{11} - C_{12})]}. \tag{31}$$

In this study, the elastic constants are obtained up to 27.5 GPa. Thus, based on the elastic data in this study and lattice parameters in Ref. [21], we calculate the coefficients (λ_2, λ_4, B, and B^*) by Eqs. (25)–(31) and Eq. (S2) in the Supplementary Material.[21] The value of $P_{\rm C}$ is assumed to be 9.6 GPa on basis of Ref. [21] rather than 10.3 GPa. The reason is that the $P_{\rm C}$ can be obtained by $\omega^2 = \omega_0^2(P/P_{\rm C} - 1)$, where ω is the frequency shift of $A_{\rm g}$ mode at each pressure, ω_0 is the frequency shift of $A_{\rm g}$ mode under ambient condition and P is the pressure. However, the $A_{\rm g}$ mode at $\sim$40 $\rm cm^{-1}$ is not observed because the low wavenumber region is not detected in our Raman scattering measurements. C_{11} and C_{12} at 9.6 GPa are calculated by the finite strain equation on basis of this study [Table 3; Eqs. (3)–(6)]. The calculated Landau model coefficients are summarized in Table 3 to compare with two previous studies.[9,21] The coefficients of the Landau potential were calculated at low temperature and at room pressure in Ref. [9], and Guennou *et al.* performed the high pressure coefficients for $SrTiO_3$.[21] However, due to lacking of elastic data, C_{11} and C_{12} are obtained by extrapolating the data of Ishidate *et al.*[23] The coefficients of the Landau potential obtained in this study are between the results of the two previous studies.[9,21] Because the reliable elastic constants are used in the present Landau model, we believe that our results provide more precise Landau potential coefficients.[9,21]

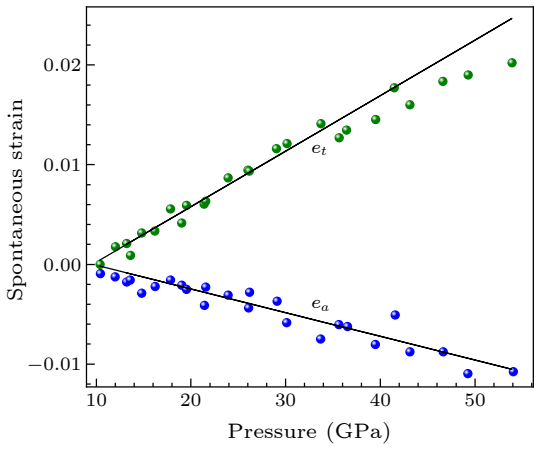

Fig. 6. Volume and tetragonal spontaneous strains e_a and e_t. The solid circles are the experimental data from Ref. [21]. The straight lines are the results on basis of calculated Landau potential in this study.

Our results have profound implications for understanding the seismic structure of the Earth's lower mantle.[52,53] Since the elastic properties of $CaSiO_3$ were poorly determined up to 20 GPa,[14,54–61] the elastic data for $SrTiO_3$ could provide critical constrains on the elastic properties of cubic and tetragonal phases of $CaSiO_3$. Previous study indicates that the Ti-bearing $CaSiO_3$ may undergo the cubic-to-tetragonal phase transition at the Earth's mid-mantle.[14] On basis of XRD data and acoustic velocity data, previous studies predicted that the transition of $CaSiO_3$ will cause 4.3% and 9.1% differences for cubic and tetragonal phases in $V_{\rm P}$ and $V_{\rm S}$ at 110 GPa and 1000 K.[13,14,59] The experimental results presented here indicate that the cubic-to-tetragonal transition of

$SrTiO_3$ will lead to 6% and 10% drops for V_P and V_S at 10.3 GPa, which is compatible with the transition of $CaSiO_3$ [Fig. 5(a)].[13] In addition, the cubic-tetragonal transition causes 0.7 and 0.3 density jumps at the transition pressure for $CaSiO_3$ and $SiTiO_3$, respectively.[14,21] The similar velocity drops and density jumps for the cubic-to-tetragonal transition of $CaSiO_3$ and $SrTiO_3$ provide promising information for using $SrTiO_3$ as an analog of $CaSiO_3$. More importantly, the calculated anisotropy on $SrTiO_3$ shows that the A_P and A_S^{PO} in anisotropy of the tetragonal phase are 5.5% and 21.7% higher than those of the cubic phase [Fig. 5(b)], respectively.

The sinking of subduction slabs into the Earth's lower mantle may cause the compositional heterogeneity leading to the observed seismic anomalies.[62] In addition, the spin transition of ferropericlase and the presence of water may be the possible reason for the seismic anomalies.[63,64] On the other hand, the previous study[14] indicates that the cubic-tetragonal phase transition of Ti-bearing $CaSiO_3$ could occur in the subduction slabs at the depth of the Earth's mid-mantle and cause the observed velocity discontinuity. On basis of the results of $SrTiO_3$, we believe that the tetragonal $CaSiO_3$ could have an extremely higher A_S^{PO} than the cubic phase. Thus, the cubic-to-tetragonal transition of $CaSiO_3$ could lead to the anomalies of the high anisotropy of V_S splitting of the Earth's mid-mantle.[53,65]

In summary, the elastic properties and phase transition of single-crystal $SrTiO_3$ have been investigated by using Brillouin scattering and Raman scattering up to 27.5 GPa at 298 K. The cubic-to-tetragonal phase transition causes abnormal changes on the elastic properties of single-crystal $SrTiO_3$ at 10.3 GPa. We find that different transition pressures of cubic-tetragonal of $SrTiO_3$ in previous studies should be caused by the different pressure transmitting media used in the different research groups. The transition also causes the softening of modulus of single crystal above 10.3 GPa. More accurate coefficients of the Landau potential are calculated based on the obtained elastic constants. Using our elasticity and Raman data, we also find that there may be a structural transition occurring at 21.7 GPa and the mechanism should be investigated in future. In addition, $SrTiO_3$ as an analog of $CaSiO_3$ indicates that the tetragonal $CaSiO_3$ has higher anisotropy than cubic phase. The presence of tetragonal Ti-bearing $CaSiO_3$ helps to explain the large A_S^{PO} of the Earth's mid-mantle.

Acknowledgments. Xinyang Li acknowledges support from China Postdoctoral Science Foundation (Grant No. 2020M670841). Fangfei Li acknowledges support from the National Key Research and Development Program of China (Grant No. 2017YFA0403704). Xinyang Li and Qiang Zhou acknowledge supports from the National Natural Science Foundation of China (Grant Nos. 12074141, 42102030, and 11974129). Fangfei Li and Liang Li acknowledge support from Jilin Provincial Science and Technology Development Project (Grant Nos. 20210402054GH and 20210509038RQ). Liang Li acknowledges support from the Program for Science and Technology of Education Department of Jilin Province (Grant No. JJKH20211036KJ), and the Fundamental Research Funds for the Central Universities.

References

[1] Frederikse H, Thurber W, and Hosler W 1964 *Phys. Rev.* **134** A442
[2] Itoh M, Wang R, Inaguma Y, Yamaguchi T, Shan Y, and Nakamura T 1999 *Phys. Rev. Lett.* **82** 3540
[3] Koonce C, Cohen M L, Schooley J, Hosler W, and Pfeiffer E 1967 *Phys. Rev.* **163** 380
[4] Burke W and Pressley R 1971 *Solid State Commun.* **9** 191
[5] Balachandran U and Eror N 1981 *J. Solid State Chem.* **39** 351
[6] Bednorz J and Müller K 1984 *Phys. Rev. Lett.* **52** 2289
[7] Kim K H, Jun J H, and Choi J S 1985 *J. Phys. Chem. Solids* **46** 1173
[8] Wang Y Q, Liu Y, Zhang M X, and Min F F 2018 *Chin. Phys. Lett.* **35** 017101
[9] Carpenter M A 2007 *Am. Mineral.* **92** 309
[10] Fischer G J, Wang Z C, and Karato S I 1993 *Phys. Chem. Miner.* **20** 97
[11] Nestola F, Korolev N, Kopylova M, Rotiroti N, Pearson D, Pamato M, Alvaro M, Peruzzo L, Gurney J, and Moore A 2018 *Nature* **555** 237
[12] Tschauner O, Huang S, Yang S, Humayun M, Liu W, Gilbert C S N, Bechtel H A, Tischler J, and Rossman G R 2021 *Science* **374** 891
[13] Sun N, Bian H, Zhang Y, Lin J F, Prakapenka V B, and Mao Z 2022 *Am. Mineral.* **107** 110
[14] Thomson A R, Crichton W A, Brodholt J P, Wood I G, Siersch N C, Muir J M R, Dobson D P, and Hunt S A 2019 *Nature* **572** 643
[15] Komabayashi T, Hirose K, Sata N, Ohishi Y, and Dubrovinsky L S 2007 *Earth Planet. Sci. Lett.* **260** 564
[16] Sun N, Mao Z, Yan S, Wu X, Prakapenka V B, and Lin J F 2016 *J. Geophys. Res.: Solid Earth* **121** 4876
[17] Ishii T, Miyajima N, Criniti G, Hu Q, Glazyrin K, and Katsura T 2022 *Earth Planet. Sci. Lett.* **584** 117472
[18] Grzechnik A, Wolf G H, and McMillan P F 1997 *J. Raman Spectrosc.* **28** 885
[19] Müller K A and Berlinger W 1971 *Phys. Rev. Lett.* **26** 13
[20] Bonello B, Fischer M, and Polian A 1989 *J. Acoust. Soc. Am.* **86** 2257
[21] Guennou M, Bouvier P, Kreisel J, and Machon D 2010 *Phys. Rev. B* **81** 054115
[22] Ishidate T and Isonuma T 1992 *Ferroelectrics* **137** 45
[23] Ishidate T, Sasaki S, and Inoue K 1988 *High Press. Res.* **1** 53
[24] Lheureux D, Polian A, Fischer M, Gauthier M, and Itié J 2000 *IEEE Ultrason. Symp.* **1** 557
[25] Hachemi A, Hachemi H, Ferhat-Hamida A, and Louail L 2010 *Phys. Scr.* **82** 025602
[26] Lytle F W 1964 *J. Appl. Phys.* **35** 2212
[27] Samara G and Giardini A 1965 *Phys. Rev.* **140** A954
[28] Yen J and Nicol M 1992 *J. Appl. Phys.* **72** 5535
[29] Wang J, Zhou Q, Guo S, Huang Y, Huang X, Wang L, Li F, and Cui T 2020 *Chin. Phys. Lett.* **37** 066201
[30] Whitfield C H, Brody E M, and Bassett W A 1976 *Rev. Sci. Instrum.* **47** 942
[31] Every A 1980 *Phys. Rev. B* **22** 1746
[32] Bell R and Rupprecht G 1963 *Phys. Rev.* **129** 90
[33] Birch F 1978 *J. Geophys. Res.: Solid Earth* **83** 1257
[34] Klotz S, Chervin J, Munsch P, and Le M G 2009 *J. Phys. D* **42** 075413
[35] Schreiber E, Anderson O L, and Soga N 1973 *Elastic Constants and their Measurements* (New York: McGraw-Hill) p 196
[36] Itié J P, Couzinet B, Dhaussy A C, Flank A M, Jaouen N, Lagarde P, and Polian A 2006 *High Press. Res.* **26** 325
[37] Dennison J R, Holtz M, and Swain G 1996 *Spectroscopy* **11** 38

[38] Nelson D G and Williamson B E 1982 *Aust. J. Chem.* **35** 715

[39] Wang X, Kunc K, Loa I, Schwarz U, and Syassen K 2006 *Phys. Rev. B* **74** 134305

[40] Zhu S C, Chen G W, Zhang D, Xu L, Liu Z P, Mao H K, and Hu Q 2022 *J. Am. Chem. Soc.* **144** 7414

[41] Wu Z J, Zhao E J, Xiang H P, Hao X F, Liu X J, and Meng J 2007 *Phys. Rev. B* **76** 054115

[42] Jiang F, Gwanmesia G D, Dyuzheva T I, and Duffy T S 2009 *Phys. Earth Planet. Inter.* **172** 235

[43] Zhang J, Li B, and Zhao Y 2008 *High Press. Res.* **28** 415

[44] Decremps F, Zhang J, Li B, and Liebermann R C 2001 *Phys. Rev. B* **63** 224105

[45] Glazer A M 1972 *Acta Crystallogr. B* **28** 3384

[46] Buchen J, Marquardt H, Schulze K, Speziale S, Boffa B T, Nishiyama N, and Hanfland M 2018 *J. Geophys. Res.: Solid Earth* **123** 7347

[47] Carpenter M A 2006 *Am. Mineral.* **91** 229

[48] Carpenter M A, Hemley R J, and Mao H K 2000 *J. Geophys. Res.: Solid Earth* **105** 10807

[49] Hemley R J, Shu J, Carpenter M, Hu J, Mao H, and Kingma K 2000 *Solid State Commun.* **114** 527

[50] Zhang Y, Fu S, Wang B, and Lin J F 2021 *Phys. Rev. Lett.* **126** 025701

[51] Salje E, Wruck B, and Thomas H 1991 *Z. Phys. B* **82** 399

[52] Ritsema J, Deuss A, van Heijst H J, and Woodhouse J H 2011 *Geophys. J. Int.* **184** 1223

[53] Waszek L, Schmerr N C, and Ballmer M D 2018 *Nat. Commun.* **9** 385

[54] Kawai K and Tsuchiya T 2015 *Geophys. Res. Lett.* **42** 2718

[55] Li L, Weidner D J, Brodholt J, Alfè D, David P G, Caracas R, and Wentzcovitch R 2006 *Phys. Earth Planet. Inter.* **155** 249

[56] Stixrude L and Lithgow-Bertelloni C 2011 *Geophys. J. Int.* **184** 1180

[57] Sinelnikov Y D, Chen G, and Liebermann R C 1998 *Phys. Chem. Miner.* **25** 515

[58] Kudo Y, Hirose K, Murakami M, Asahara Y, Ozawa H, Ohishi Y, and Hirao N 2012 *Earth Planet. Sci. Lett.* **349** 1

[59] Gréaux S, Irifune T, Higo Y, Tange Y, Arimoto T, Liu Z, and Yamada A 2019 *Nature* **565** 218

[60] Li B, Kung J, and Liebermann R C 2004 *Phys. Earth Planet. Inter.* **143** 559

[61] Immoor J, Miyagi L, Liermann H P, Speziale S, Schulze K, Buchen J, Kurnosov A, and Marquardt H 2022 *Nature* **603** 276

[62] van der Hilst R D and Kárason H 1999 *Science* **283** 1885

[63] Shahnas M H, Yuen D A, and Pysklywec R N 2017 *Earth Planet. Sci. Lett.* **458** 293

[64] Zhuang Y, Gan B, Cui Z, Tang R, Tao R, Hou M, Jiang G, Popescu C, Garbarino G, Zhang Y, and Hu Q 2022 *Sci. Bull.* **67** 748

[65] French S and Romanowicz B A 2014 *Geophys. J. Int.* **199** 1303

Supplementary Material: Abnormal Elastic Changes for Cubic-Tetragonal Transition of Single-Crystal $SrTiO_3$

Caizi Zhang(张才姿)[1], Fangfei Li(李芳菲)[1], Xinmiao Wei(魏鑫苗)[1], Mengqi Guo(郭梦琪)[1], Yingzhan Wei(魏颖展)[1], Liang Li(李亮)[1], Xinyang Li(李新阳)[1]*, and Qiang Zhou(周强)[1,2]

[1]*State Key Laboratory of Superhard Materials, Jilin University, Changchun 130012, China*
[2]*Synergetic Extreme Condition User Facility, Jilin University, Changchun 130012, China*

*Corresponding author. Email: lixinyang@jlu.edu.cn

Landau potential can be expressed by Eq. (24).[9] The equilibrium values of the spontaneous strains can be obtained by $\frac{\partial G}{\partial e} = 0$. Using the equilibrium values of the spontaneous strains replace themselves, a renormalized 246 Landau potential $\left(\frac{A^*}{2}\right)Q^2+\left(\frac{B^*}{4}\right)Q^4+(\frac{C}{6})Q^6$ can be obtained. The renormalized coefficients express as follow:

$$A^* = A\Theta_S\left[\coth\frac{\Theta_S}{T}-\coth\frac{\Theta_S}{T_C}\right]-\frac{2\lambda_2 P}{\frac{1}{3}(C_{11}^0+2C_{12}^0)}, \tag{S1}$$

$$B^* = B-\frac{2\lambda_2^2}{\frac{1}{3}(C_{11}^0+2C_{12}^0)}-\frac{8\lambda_4^2}{\frac{1}{2}(C_{11}^0-C_{12}^0)}. \tag{S2}$$

λ_2 can be determined by $A^* = 0$, which also can define the phase boundary in P-T diagram:

$$P_C = A\Theta_S\frac{K}{2\lambda_2}\left[\coth\frac{\Theta_S}{T}-\coth\frac{\Theta_S}{T_C}\right]. \tag{S3}$$

The λ_2 is not affected by the pressure when the temperature is higher than 200 K,[9] and the λ_2 can be obtained by a least-square fit with K_0 for Eq. (S3). However, the above Landau model is not suitable for the pressure-induced phase transition.[21] Therefore, Guennou *et al*. developed a Landau model with respect to the pressure-induced phase transition.[21] The order parameters above the transition pressure can be given by:

$$Q^2 = \frac{1}{2C}\left[-B^*+\sqrt{B^{*2}+4\frac{2\lambda_2}{K}C(P-P_C)}\right]. \tag{S4}$$

Guennou *et al*. simplified the order parameters by hypothesis the $C = 0$, Then the volume strain and tetragonal strain as a function of pressure can be expressed as Eqs. (29) and (30). Combined with Eqs. (25)-(28), and (31), the Landau coefficients λ_2, λ_4, B and B* can be calculated.[21]